

# NUMERICAL INVESTIGATION OF INTERNAL FLOWS WITH SUB-COOLED NUCLEATE BOILING

Fukuda, K., Iqbal, O., Barron, R.M.\* and Balachandar, R.

\*Author for correspondence

Department of Mechanical, Automotive and Materials Engineering  
University of Windsor  
Windsor, ON  
Canada  
E-mail: az3@uwindsor.ca

## ABSTRACT

This paper discusses numerical simulations of sub-cooled nucleate boiling in a duct using Reynolds Stress Model (RSM) and conjugate heat transfer (CHT). The predictions of flow characteristics and distributions of interfacial area concentration (IAC), Sauter mean diameter (SMD), temperature of liquid and void fraction of gas are investigated using the above methods. The RSM turbulence model is used in the simulations to incorporate anisotropic turbulence, which has been reported in experimental studies, where it has been observed that the flow is affected by the drag of bubbles nucleating at a heater block. The heat flux, which leads to phase change of the fluid, has been applied in two different ways. One implementation involves the fluid-only domain with a particular boundary providing constant heat flux, whereas, in the other case, the solid duct has been made part of the computational domain and the fluid has been heated via CHT. The study first focuses on investigating the mean and fluctuating velocity components over the heated section of the domain. It is found that the bubbly layer is predicted thinner in the solid-fluid case than the fluid-only case. Amount of heat flux added to the coolant is higher in the case where the computational domain is limited to the fluid only. This results in a relatively larger amount of void fraction directly above the heated section.

## NOMENCLATURE

$c_p$	[J/kg·K]	Specific heat
$C_D$	[‐]	Drag coefficient
$d_l$	[m/rad]	Calibration constant
$d_w$	[m]	Bubble departure diameter
$D_h$	[m]	Hydraulic diameter
$Eo$	[‐]	Eötvös number
$f$	[Hz]	Bubble departure frequency
$f_d$	[‐]	Drag correction factor
$F$	[N]	Force
$F_A$	[‐]	Area coefficient
$G$	[m/s <sup>2</sup> ]	Gravitational acceleration
$h_{fg}$	[J/kg]	Latent heat
$k$	[W/m·K]	Thermal conductivity
$K_{dry}$	[‐]	Wall dryout area fraction
$K_{quench}$	[‐]	Bubble influence wall area fraction
$l_{ca}$	[m]	Interaction length scale
$n_P$	[‐]	Correction exponent
$N$	[‐]	Nucleation site number density
$N$	[site/m <sup>2</sup> ]	Average cavity density

$p$	[bar]	Pressure
$\dot{q}$	[kW/m <sup>2</sup> ]	Heat transfer rate
$R$	[‐]	Gas constant per molecular weight
$R_{ij}$	[‐]	Reynolds stress
$Re$	[‐]	Reynolds number
$R_c$	[m]	Critical cavity radius
$t^+$	[‐]	Non-dimensional wall temperature function
$t_w$	[sec]	Waiting time
$T$	[K]	Temperature
$U^*$	[m/s]	Frictional velocity
$U_i$	[m/s]	Component of velocity
$U_r$	[m/s]	Relative velocity
$X$	[m]	X-direction
$Y$	[m]	Y-direction
$Z$	[m]	Z-direction
$\alpha$	[‐]	Volume fraction
$\theta$	[rad]	Wall contact angle
$\lambda'$	[m]	Cavity length scale
$\mu$	[rad]	Wall contact angle scale
$\mu_c$	[Pa·s]	Dynamic viscosity
$\rho$	[kg/m <sup>3</sup> ]	density
$\rho^+$	[‐]	Non-dimensional density function
$\sigma$	[N/m]	Surface tension
Special characters		
$\bar{‐}$		Time-averaged
$\tilde{‐}$		Phase-averaged
$,$		Fluctuation component
Subscripts		
$c$		Continuum (liquid) phase
$conv$		Convection
$d$		Dispersed (gas) phase
$D$		Drag
$evap$		Evaporation
$i$		x-component
$j$		y-component
$k$		z-component
$L$		Lift
$quench$		Quenching
$sat$		Saturation
$sub$		Sub-cooling
$TD$		Turbulent dispersion
$VM$		Virtual mass
$w$		Wall
$0$		Reference

## INTRODUCTION

Accurate prediction of the rate of heat rejection via convective cooling is vital for the optimization of various thermal systems. One such application is an automotive cooling circuit where more than 50% of the heat generated as a result of

combustion is convected away by engine coolant [1]. Moreover, there are regions around the combustion chamber where the liquid-solid interface temperatures could fall within the transition boiling regime, thereby limiting the rate of heat transfer. Careful tuning of the coolant flow rate over heated walls and fully utilizing the latent heat of vaporization in the nucleate boiling regime can significantly enhance the rate of heat rejection with little or no penalty on pumping energy. This, however, requires a detailed understanding of the temporal evolution of the multiphase flow field. The current study documents a novel approach to computationally model the unsteady internal flow with sub-cooled nucleate boiling utilizing a wall boiling model. The physics and domain discretization of internal steady and transient flows have been very well documented in the literature. However, phase change which is inherently a transient phenomenon poses a greater challenge in discretizing the flow domain to capture the flow behavior of each of the phases simultaneously. In this regard, numerical studies documenting discretization techniques and modeling requirements are rather scarce.

In the automotive industry, a number of studies on flow and heat transfer in the cooling circuit have been reported [1-6]. The majority of these works have considered the forced convection heat transfer to simulate the flow and heat transfer regimes, while a few others have applied a boiling model in their considerations. The boiling model which is used in these studies is adapted from the Rohsenow boiling correlation [7] with the volume of fluid (VOF) multiphase method where the correlation is originally found from pool boiling experiments. A number of new and/or modified correlations based on the combinations of fluids and conditions of the solids (surface roughness, density, etc.) have been reported and the appropriate correlation has to be chosen for the modeling [8].

Another option is to implement a sub-cooled flow boiling model which is commonly employed in the field of nuclear reactor and its safety studies [9-11]. This model uses the Eulerian multiphase method where the bubbles are considered as dispersed particles mixed in a liquid which is treated as a continuum phase. Every single process of boiling is modeled to predict the frequency of nucleation, including size of bubbles at departure, rate of evaporation, forces acting on the interface of continuum and dispersed phases, etc. Unlike a mixture model, the Eulerian multiphase method calculates the mass, momentum, energy and volume fraction for each phase and couples them at their interfaces, thus the analysis of liquid and vapor flow can easily be conducted. Numerical models for wall boiling have been proposed by a number of researchers based on analytical and experimental studies and have been improved over several decades. For validation purposes, the experiments conducted in simple geometries are often used to evaluate the numerical models. In general, there are experiments in a circular pipe, rectangular duct, annulus pipe either in horizontal or vertical orientation heated by one side of the surfaces or a part of the surface through a heating block [9, 10]. Among these experimental works, Ramstorfer et al. [12] have conducted experiments of sub-cooled flow boiling in a square cross-section duct with an aluminum heater block installed at the bottom base to investigate the flow characteristics for

various bulk velocities and heat fluxes. In the case of lower bulk velocity in their study, the results show stronger influence of bubble nucleation along the heated surface on the velocity profiles and fluctuations. Results also suggest that the velocity fluctuation profiles in streamwise and normal directions are anisotropic in nature.

To achieve accurate predictions of nucleate boiling in numerical simulations, validation with experimental works is mandatory. In numerical studies, for simplicity, it is common to assume a constant heat flux at the boundary of the heating surface and utilize a k- $\epsilon$  turbulence model in a two-dimensional (2D planar or axisymmetric) domain where the grids are mostly structured and uniformly distributed [11]. The difficulty of capturing the profiles of streamwise velocity and the distributions of interfacial area concentration (IAC), Sauter mean diameter (SMD), temperature of liquid and void fraction of gas near the heating wall is often discussed in these numerical works. However, the experiment results of Ramstorfer et al. [12] bring attention to the point that the isotropic assumption associated with the k- $\epsilon$  turbulence model is likely inappropriate since the turbulence is anisotropic. This also adds to the concern that the boiling flow is three-dimensional (3D). One of the industrial applications where the nucleate boiling models are used is the internal combustion engine's cooling jacket, which is highly 3D. Therefore, detailed 3D flow and heat transfer characteristics need to be analyzed, but these models need to be validated in simple geometries. Additionally, issues regarding the effect of the mesh on velocity profile and distributions of IAC, SMD, temperature of liquid and void fraction of gas should be investigated. Finally, a conjugate heat transfer (CHT) simulation has also been conducted to allow the heat to also distribute within the solid part and the results are compared with the constant heat flux wall boundary simulation.

## NUMERICAL MODELING

### Governing Equations

Phase change (boiling) introduces anisotropy of turbulence which is better captured using the Reynolds stress model (RSM) [13] compared to the k- $\epsilon$  turbulence model which assumes the turbulence as isotropic. A two-layer all  $y^+$  wall treatment is used to resolve the boundary layer near the walls. The continuity and energy equations for the continuum phase are

$$\frac{\partial}{\partial t}(\bar{\alpha}_c \rho_c) + \nabla \cdot (\bar{\alpha}_c \rho_c \tilde{U}_c) = 0 \quad (1)$$

$$\frac{\partial}{\partial t}(\bar{\alpha}_c \rho_c \tilde{U}_c) + \nabla \cdot (\bar{\alpha}_c \rho_c \tilde{U}_c \times \tilde{U}_c) = -\bar{\alpha}_c \nabla \tilde{p} + \nabla \cdot (-\bar{\alpha}_c \rho_c \tilde{R}_{c,ij}) + F \quad (2)$$

where  $R_{ij}$  are the Reynolds stresses,  $\bar{u}_i' \bar{u}_j'$ , and the transport equation for  $R_{ij}$  is given as:

$$\begin{aligned} \frac{\partial}{\partial t}(\bar{\alpha}_c \rho_c \tilde{R}_{c,ij}) + \nabla \cdot (\bar{\alpha}_c \rho_c \tilde{U}_c \tilde{R}_{c,ij}) &= -\bar{\alpha}_c \rho_c \left( \tilde{R}_{c,ik} \frac{\partial \tilde{U}_{c,j}}{\partial x_k} + \tilde{R}_{c,jk} \frac{\partial \tilde{U}_{c,i}}{\partial x_k} \right) \\ &+ \nabla \cdot (\bar{\alpha}_c \mu_c \nabla \cdot \tilde{R}_{c,ij}) + \Pi_{R,ij} + \nabla \cdot (\bar{\alpha}_c \rho_c \bar{u}_i' \bar{u}_j' \bar{u}_k') + \bar{\alpha}_c \bar{p} \nabla \bar{u}_i' - \bar{\alpha}_c \rho_c \tilde{\varepsilon}_{ij}. \end{aligned} \quad (3)$$

Considering the bubbles as dispersed particles in the continuum phase, the turbulence response model developed by Issa and Oliveira [14] and Behzadi et al. [15] is used as a dispersed phase turbulence model instead of using the Reynolds-Averaged Navier-Stokes (RANS) turbulence models.

### Boiling Models

Sub-cooled wall boiling is used in the current study. This model is based on the RPI model proposed by Kurul and Podowski [16] where the total heat flux due to the wall boiling is the summation of convection, evaporation and quenching heat fluxes,

$$\dot{q}_w = \dot{q}_{conv} + \dot{q}_{evap} + \dot{q}_{quench} \quad (4)$$

The convective heat flux of the continuum phase is computed by

$$\dot{q}_{conv} = (1 - K_{dry})(1 - K_{quench}) \frac{\rho_c c_p c U^*}{t_c^+} (T_w - T_c) \quad (5)$$

whereas the dispersed phase convective heat flux is expressed as

$$\dot{q}_{d_{conv}} = K_{dry} \frac{\rho_d c_{pd} U_d^*}{t_d^+} (T_w - T_d) \quad (6)$$

where  $K_{dry}$  is the wall dryout area fraction of the gas phase [17],  $T$  is the temperature,  $U^*$  is the frictional velocity, and  $t^+$  is a non-dimensional value determined by temperature wall function, where subscript c and d define liquid and gas phases, respectively, and w refers to wall.  $K_{quench}$  is the bubble influence wall area fraction which is defined by Kurul and Podowski [16] as

$$K_{quench} = F_A N \frac{\pi d_w^2}{4} \quad (7)$$

where  $F_A$  is an area coefficient set to 2.0 by default,  $N$  is the nucleation site number density and  $d_w$  is the bubble departure diameter. Since high wall superheats ( $\Delta T_w = 10 - 35$  K) are observed in the experiment, the Hibiki Ishii model [18] is selected to predict the nucleation site number density,  $N$ :

$$N = \bar{N} \left( 1 - e^{-\frac{\theta^2}{8\mu^2}} \right) \left( e^{[(c_0 + c_1 \rho^+ + c_2 \rho^{+2} + c_3 \rho^{+3}) \frac{\lambda'}{R_c}]} - 1 \right) \quad (8)$$

where

$$R_c = \frac{2\sigma \left( 1 + \frac{\rho_d}{\rho_c p} \right)}{e^{\left[ \frac{h_{fg}(T_d - T_{sat})}{RT_d T_{sat}} \right]} - 1} \quad (9)$$

and

$$\rho^+ = \log_{10} \left( \frac{\rho_c - \rho_d}{\rho_d} \right). \quad (10)$$

Paired with the Hibiki Ishii model, the Kocamustafaogullari bubble departure diameter model [19], which is calibrated for a wide range of system pressures, is used to determine the size of bubbles departing from the heating surface,

$$d_w = d_1 \theta \sqrt{\frac{\sigma}{g(\rho_c - \rho_d)}} \left( \frac{\rho_c - \rho_d}{\rho_d} \right)^{0.9}. \quad (11)$$

Here,  $d_1$  is a calibration constant and  $\theta$  is a wall contact angle for the working fluid in the system.

The Del Valle Kenning bubble induced quenching heat transfer coefficient [20] is used to obtain the quenching heat flux,

$$\dot{q}_{quench} = K_{quench} (2f) \sqrt{\frac{\rho_c c_p k_c t_w}{\pi}} (T_w - T_c) \quad (12)$$

where  $t_w$  is the waiting time since the departure of a bubble until the nucleation of the next one and  $f$  is the bubble departure frequency which is modeled by Cole [21]

$$f = \sqrt{\frac{4 g (\rho_c - \rho_d)}{3 d_w \rho_c}}. \quad (13)$$

The evaporation heat flux is estimated by [16]

$$\dot{q}_{evap} = (1 - K_{dry}) f N \left( \frac{\pi d_w^3}{6} \right) \rho_d h_{fg}. \quad (14)$$

The rate of evaporation, which is the rate of conversion from liquid to gas phase per unit wall area, can be found as [16]

$$\dot{m}_{evap} = \frac{\dot{q}_{evap}}{h_{fg}} = (1 - K_{dry}) f N \left( \frac{\pi d_w^3}{6} \right) \rho_d. \quad (15)$$

### Interfacial Force Models

Forces acting on the interface of the continuum and dispersed phases are modeled and included in the continuum phase energy equation (2) through the term  $F$ . In sub-cooled flow boiling, four forces are commonly considered in the simulation: drag, lift, virtual mass and turbulent dispersion forces, i.e.

$$F = F_D + F_L + F_{VM} + F_{TD}. \quad (16)$$

Based on the Eötvös number,  $Eo$ , it is found that  $Eo = 0.35 < 1.0$  where the surface tension force is greater than the buoyancy force; therefore, the Schiller-Naumann model [22] is chosen to calculate the single bubble drag force coefficient and the Richardson Zaki model [23] is used to correct the drag force for moderate concentration of bubbles.

The single bubble drag coefficient is determined based on bubble size Reynolds number in the Schiller-Naumann model,

$$C_D = \begin{cases} \frac{24}{Re_d} (1 + 0.15 Re_d^{0.687}) & \text{for } 0 < Re_d \leq 1000 \\ 0.44 & \text{for } Re_d > 1000 \end{cases} \quad (17)$$

where

$$Re_d = \frac{\rho_c |U_r| l_{cd}}{\mu_c}. \quad (18)$$

The interaction length scale,  $l_{cd}$ , in the above calculation is the diameter of bubbles, which is obtained from the computed SMD.

**Table 1** Richardson Zaki drag correction [23]

Range	Correction Exponent: $n_D$
$Re_d < 0.2$	-8.3
$0.2 < Re_d < 1.0$	$1 - \left( 8.7 + 35 \frac{d_w}{D_h} \right) Re_d^{-0.03}$
$1.0 < Re_d < 200$	$1 - \left( 8.7 + 36 \frac{d_w}{D_h} \right) Re_d^{-0.1}$
$200 < Re_d < 500$	$1 - 8.9 Re_d^{-0.1}$
$Re_d > 500$	-3.78

The drag coefficient correction factor for a moderate cloud of bubbles is a function of liquid phase void fraction exponent

$n_D$  which is obtained from the correlation between single and concentric bubble terminal velocities,

$$f_D = \alpha_c^{n_D}. \quad (19)$$

The exponent  $n_D$  is determined based on single bubble Reynolds number as shown in the Table 1.

## NUMERICAL SETUPS

In this study, the computational domain and fluid flow conditions are a replica of what has been reported by Ramstorfer et al. [12]. The experiments were conducted in a square duct (36 mm x 36 mm) with a 65 mm (L) x 10 mm (W) aluminum heater block installed at the bottom of the duct which is made of polytetrafluoroethylene (PTFE). The working fluid for this study is a water/ethylene glycol 60/40 vol.% mixture. The experiments were carried out at the system pressure of 1.5 bar (absolute). The bulk velocity of the fluid ranged from 0.1 to 0.8 m/s. The temperature of the liquid entering the testing section was maintained at a sub-cooled temperature of 22 K. The heat flux applied at the bottom of the heater block varied from 0.0 to 461 kW/m<sup>2</sup>.

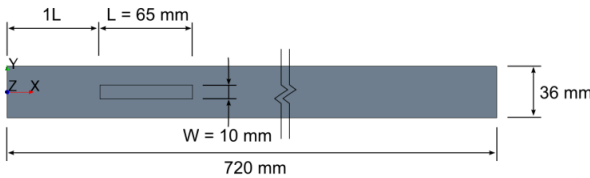


**Figure 1** Top view of computational domain and its dimensions

In the current work, Star-CCM+ v.8.06 is used to carry out the numerical investigations of the wall boiling model. In this study, the lowest bulk velocity,  $u_b = 0.1$  m/s, and two heat flux values,  $q_w = 148$  and  $247$  kW/m<sup>2</sup>, cases are simulated. The lowest bulk velocity is chosen because the effect of bubble nucleation is more significant on the velocity and its fluctuation near the heating wall. For the computational domain of fluid, a 720 mm long duct with 36 mm wide square cross-section is created (Figure 1). The leading edge of the heating section is located 1L (65 mm) downstream from the inlet boundary and set in the middle from the side walls. The wall boundaries at the top and side walls are set to no-slip adiabatic boundary conditions. The aluminum heater block is kept in an insulating material with one of its face exposed to the fluid domain. A constant heat flux is specified on the face opposite to the face exposed to fluid. The inlet of the computational domain is defined with velocity and turbulence quantities profiles computed separately from a stand-alone flow only simulation using the same duct. The temperature of liquid at the inlet is kept at 22 K below the saturation temperature at the given system pressure. The pressure outlet boundary is set to the system pressure of 1.5 bar (absolute).

Two different cell counts are generated in the fluid-only domain case where constant heat flux is applied in the heated section. The solid-fluid model is discretized separately to carry out conjugate heat transfer (CHT) simulations. The near-wall region is discretized fine enough to ensure the  $y^+$  lies below 1.0 in single phase adiabatic flow. Different growth rates (1.04 and 1.1) are applied at the boundary layer. The total number of cells

in each case becomes 0.452 million (fluid-only domain) for growth factor of 1.1, 0.855 million (fluid-only domain) for growth factor of 1.04, and 1.23 million cells for growth factor of 1.1 in the CHT case, as summarized in Table 2. It is established that the approaching flow is fully developed and the profiles remain the same at the leading edge of the heater block to make sure the distance from the inlet does not affect the results. The velocity profiles of zero heat flux case for each mesh are validated with the experiment of Ramstorfer et al. [12] and are verified to match well with their results.

**Table 2:** Summary of case studies

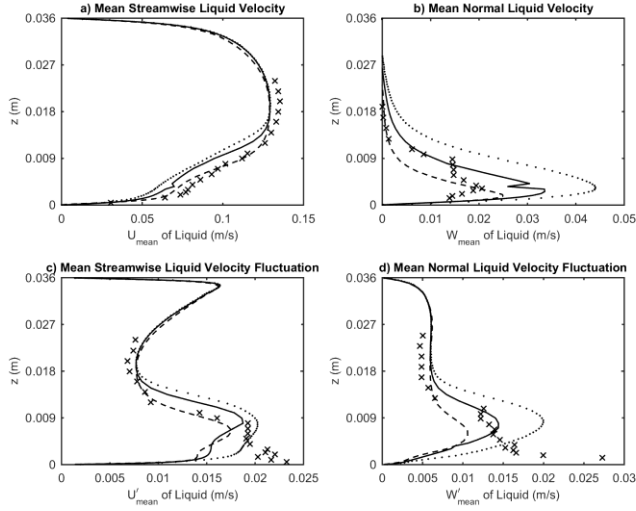
	Fluid-only model		Solid-fluid model
	Case 1	Case 2	Case 3
Cell count	0.452 million	0.855 million	1.23 million
Heat flux	148 and 247 kW/m <sup>2</sup>		
Bulk velocity	0.1 m/s		
System pressure	1.5 bar		

## RESULTS AND DISCUSSIONS

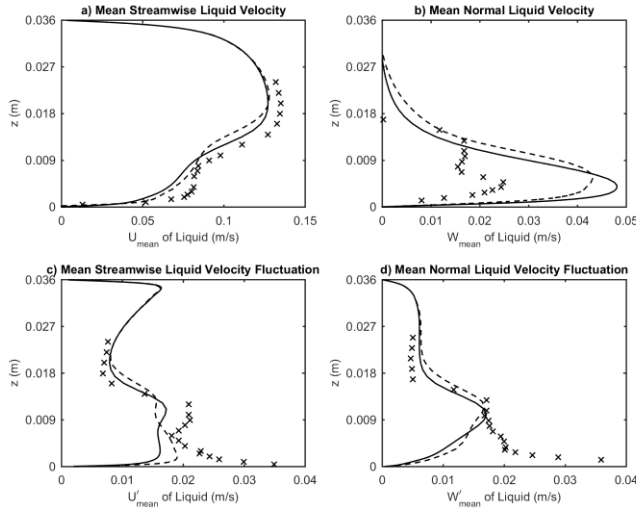
Boiling is inherently a transient phenomenon, hence, time dependent momentum and energy equations are solved to capture the flow and thermal transients. The heat flux is gradually ramped up for flow and thermal stability in the solution. 10,000 samples of each parameter of interest are recorded at the rate of 1000 Hz. The root mean square (RMS) of streamwise and normal velocities are estimated by taking the square root of computed Reynolds stresses ( $u' = \sqrt{u'u'}$  and  $w' = \sqrt{w'w'}$ , respectively).

Figure 2 shows time-averaged streamwise and wall normal velocity profiles (mean and fluctuating) of all three cases for a given heat flux ( $q_w = 148$  kW/m<sup>2</sup>). The experimental results are shown with cross symbols whereas Case 1, Case 2, and Case 3 are shown as solid, dotted and dashed lines, respectively. The location  $Z = 0.0$  m is where the heat flux is applied and  $Z = 0.036$  m is where the top surface of the duct is located. It is seen that the mean streamwise velocity profile follows the same trends as test data, however, numerical results under-predict the magnitude in the range of  $0.0 < Z < 0.015$  m. On the other hand, the mean normal velocity and its fluctuation (RMS velocity) are over-predicted in the same range of wall normal direction for Cases 1 and 2. The peaks of normal velocity and RMS velocity in the fluid-only cases are shifted away from the wall compared to the experiment results. The fine mesh (Case 2) tends to overestimate the peaks, whereas the results of the coarse mesh come closer to the experiment. Compared to the fluid-only cases, the solid-fluid cases show mean streamwise velocity and RMS velocity that have a better match with the experiment. The peak of mean normal velocity is closer to that of experiment and the location of the peak is also predicted well. The normal RMS velocity is under-predicted in Case 3 while a better match is observed at the core of the duct. Similarly, the CHT case can predict the streamwise RSM velocity well near the center of the duct, however, the peak of streamwise RMS velocity near the wall is better captured in Case 2. As observed in all cases, it is difficult to capture the peak of RMS velocity next to the heating surface even though the grid is refined near the walls. However,

the mean velocity profiles are improved when the heat transfer through the solids are included in the simulations.



**Figure 2** Mean streamwise and normal velocities and RMS for  $q_w = 148 \text{ kW/m}^2$  (Case 1: —, Case 2: ...., Case 3: ---, Experiment: XXX)



**Figure 3** Mean streamwise and normal velocities and RMS for  $q_w = 247 \text{ kW/m}^2$  (Case 1: —, Case 3: ---, Experiment: XXX)

Similarly, the results of higher heat flux case ( $q_w = 247 \text{ kW/m}^2$ ) are presented in Figure 3. The fluid-only simulation with the coarse mesh (Case 1) and the solid-fluid simulation (Case 3) are compared. It can be seen that there is a small deviation from the experimental results in the mean streamwise velocity whereas there is a large difference in the mean normal velocity in Case 1. Both streamwise and normal RMS velocities are under-predicted near the heating surface but have better prediction near and above the centre-line of the duct. In Case 3, the mean streamwise velocity profile near the heating surface is slightly better than the other case, but it loses accuracy towards the peak near the center of the duct. The magnitude of the peak normal velocity is smaller compared to Case 1; however, the peak is still over-estimated. The normal RMS velocity profile is very similar to the fluid-only case whereas the streamwise RMS

velocity profile shows the peak near the wall is larger than the second peak away from the wall, but both peaks are underpredicted. The same trend is observed in the normal RMS velocity profiles.

The peak near the heated wall in the RMS velocities are difficult to capture in the simulations. There is an improvement when both the solid and fluid are modeled, but the magnitudes of the peaks do not reach to that of the experiments.

Finally, the distributions of IAC, SMD, temperature of liquid and void fraction of gas for each case are presented in Figure 4 and Figure 5. Since there is no experimental data provided for these parameters in the work of Ramstorfer et al. [12], the computed results cannot be validated. Nevertheless, it is worthwhile to assess the performance of each model with respect to these important parameters in flow boiling.

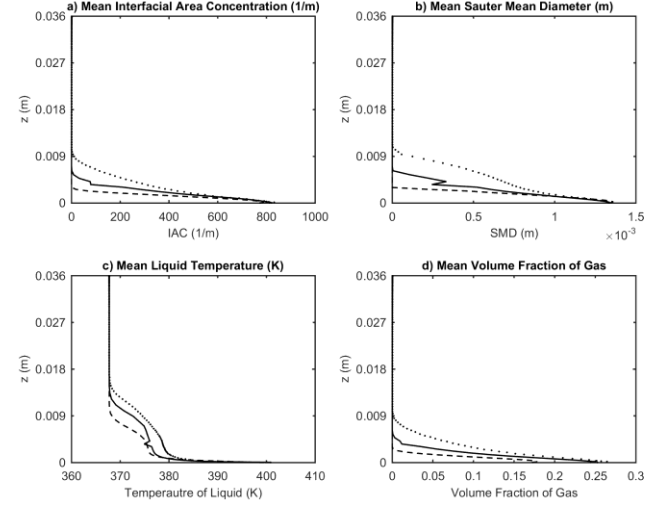


**Figure 4** Mean IAC, SMD, temperature of liquid and void fraction of gas for  $q_w = 148 \text{ kW/m}^2$  (Case 1: —, Case 2: ...., Case 3: ---)

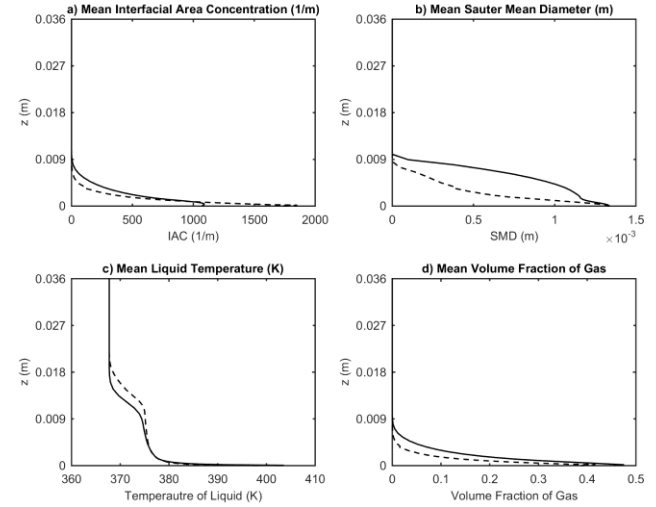


**Figure 5** Mean IAC, SMD, temperature of liquid and void fraction of gas for  $q_w = 247 \text{ kW/m}^2$  (Case 1: —, Case 3: ---)

Overall, the fluid-only cases predict a much thicker bubbly layer compared to the solid-fluid model. For example, the mean

of void fraction of gas is found to be zero at around  $Z = 0.01$  m in Cases 1 and 2 with the heat flux of  $148 \text{ kW/m}^2$  whereas zero void fraction of gas is observed at around  $Z = 0.003$  m for Case 3. Similar conclusions can be drawn for the higher heat flux cases. The thickness of the bubbly layer can be correlated with the strong normal velocities predicted by the fluid-only case. The fine mesh simulation shows a stronger upward flow and thicker layer compared to the coarse mesh and fluid-solid case. Another possible reason for thinner bubbly layers in the fluid-solid model is because the temperature of the heated surface changes over the events of bubble nucleation, which results in fluctuation of heat flux at the surface. For fluid-only cases, the constant heat flux is forced at the heating surface; therefore, there is more opportunity to transfer the heat to the fluid next to the heating area. Hence, the differences are possibly captured only in an unsteady simulation but not in a steady simulation.

## CONCLUSION

Sub-cooled flow boiling in a square duct for two heat fluxes is numerically investigated and validated with the experimental works reported by Ramstorfer et al. [12]. The RSM is used as a turbulence model to capture the anisotropic turbulence in boiling flow. Conjugate heat transfer simulations are also conducted to compare the results with the no solid case. The RSM turbulence model is able to capture the anisotropic turbulence as expected, which is not possible using two-equation models [11], but the peak near the heated wall is not well predicted by either the fluid-only or the fluid-solid model. However, the solid-fluid case can capture the trends and magnitudes of the mean velocities better than the fluid-only case. Distributions of IAC, SMD, temperature of liquid and void fraction of gas are also analyzed for each case. The thickness of the bubbly layer is found to be thicker in the fluid-only case than the solid-fluid case. This is because the heat flux at the surface of the heating block oscillates due to the periodic bubble nucleation at the surface, whereas constant heat flux is assigned at the boundary for the fluid-only case.

## ACKNOWLEDGEMENT

This research is funded through the NSERC IPS program. Simulations were made possible by the facilities of SHARCNET ([www.sharcnet.ca](http://www.sharcnet.ca)) and Compute/Calcul Canada.

## REFERENCES

- [1] Fontanesi, S., Cicalese, G., and Tiberi, A. Combined in-Cylinder / CHT Analyses for the Accurate Estimation of the Thermal Flow Field of a High Performance Engine for Sport Car Applications. *SAE Technical Paper 2013-01-1088*, 2013.
- [2] Kruger, M., Kessler, M.P., Ataides, R., De La Rosa Siqueira, C., Dos Reis, M.V.F., Mendes, A.S., Tomoyose, R., and Argachoy, C. Numerical Analysis of Flow at Water Jacket of an Internal Combustion Engine. *SAE Technical Paper 2008-01-0393*, 2008.
- [3] Dong, F., Fan, Q., Cai, Y., Jiang, S., Guo, C., Watanabe, N., and Lee, W.-T. Numerical Simulation of Boiling Heat Transfer in Water Jacket of DI Engine. *SAE Technical Paper 2010-01-0262*, 2010.
- [4] Fontanesi, S., and McAssey, E. Experimental and Numerical Investigation of Conjugate Heat Transfer in a HSDI Diesel Engine Water Cooling Jacket. *SAE Technical Paper 2009-01-0703*, 2009.
- [5] Fontanesi, S., and Giacopini, M. Multiphase CFD-CHT Optimization of the Cooling Jacket and FEM Analysis of the Engine Head of a V6 Diesel Engine. *Applied Thermal Engineering*, 52(2), pp. 293-303, 2013.
- [6] Iqbal, O., Arora, K., and Sanka, M. Thermal Map of an IC Engine Via Conjugate Heat Transfer: Validation and Test Data Correlation. *SAE International Journal of Engines*, 7(1), pp. 366-374, 2014.
- [7] Rohsenow, W.M. Boiling. *Annual Review of Fluid Mechanics*, 3(1), pp. 211-236, 1971.
- [8] Jabardo, J.M.S., Silva, E.F.D., Ribatski, G., and Barros, S.F.D. Evaluation of the Rohsenow Correlation through Experimental Pool Boiling of Halocarbon Refrigerants on Cylindrical Surfaces. *Journal of the Brazilian Society of Mechanical Sciences and Engineering*, 26, pp. 218-230, 2004.
- [9] Yu, W., Hull, J.R., France, D.M., and Ramamoorthy, V.K.V. Small-Channel Flow Boiling of One-Component Fluids and an Ethylene Glycol/Water Mixture. *Experimental Heat Transfer*, 18(4), pp. 243-257, 2005.
- [10] Yun, B.J., Bae, B.U., Euh, D.J., Park, G.C., and Song, C.H. Characteristics of the Local Bubble Parameters of a Subcooled Boiling Flow in an Annulus. *Nuclear Engineering and Design*, 240(9), pp. 2295-2303, 2010.
- [11] Shademan, M., Balachandar, R., and Barron, R. CFD Simulation of Boiling Heat Transfer Using OpenFOAM. ASME 2014 International Mechanical Engineering Congress and Exposition, ASME, Montreal, Quebec, Canada, p. 8, 2014.
- [12] Ramstorfer, F., Steiner, H., and Brenn, G. Modeling of the Microconvective Contribution to Wall Heat Transfer in Subcooled Boiling Flow. *International Journal of Heat and Mass Transfer*, 51(15–16), pp. 4069-4082, 2008.
- [13] Cokljat, D., Slack, M., Vasquez, S.A., Bakker, A., and Montante, G. Reynolds-Stress Model for Eulerian Multiphase. *Progress in Computational Fluid Dynamics*, 6(1-3), pp. 168-178, 2006.
- [14] Issa, R.I., and Oliveira, P.J. Numerical Prediction of Phase Separation in Two-Phase Flow through T-Junctions. *Computers & Fluids*, 23(2), pp. 347-372, 1994.
- [15] Behzadi, A., Issa, R.I., and Rusche, H. Modelling of Dispersed Bubble and Droplet Flow at High Phase Fractions. *Chemical Engineering Science*, 59(4), pp. 759-770, 2004.
- [16] Kurul, N., and Podowski, M.Z. Multidimensional Effects in Forced Convection Subcooled Boiling. Proc. Ninth International Heat Transfer Conference, Aug 19-24, pp. 21-26, 1990.
- [17] Weisman, J., and Pei, B.S. Prediction of Critical Heat Flux in Flow Boiling at Low Qualities. *International Journal of Heat and Mass Transfer*, 26(10), pp. 1463-1477, 1983.
- [18] Hibiki, T., and Ishii, M. Active Nucleation Site Density in Boiling Systems. *International Journal of Heat and Mass Transfer*, 46(14), pp. 2587-2601, 2003.
- [19] Kocamustafaogullari, G. Pressure Dependence of Bubble Departure Diameter for Water. *International Communications in Heat and Mass Transfer*, 10(6), pp. 501-509, 1983.
- [20] Del Valle, V.H., and Kenning, D.B.R. Subcooled Flow Boiling at High Heat Flux. *International Journal of Heat and Mass Transfer*, 28(10), pp. 1907-1920, 1985.
- [21] Cole, R. A Photographic Study of Pool Boiling in the Region of the Critical Heat Flux. *AICHE Journal*, 6(4), pp. 533-538, 1960.
- [22] CD-adapco. User Guide Star-CCM+ Version 8.06. 2013.
- [23] Richardson, J.F., and Zaki, W.N. Sedimentation and Fluidisation: Part 1. *Chemical Engineering Research and Design*, 75, Supplement, pp. S82-S100, 1997.